Ahmed, J., Constantine, J.A., and Dunne, T., 2019, The role of sediment supply in the adjustment of channel sinuosity across the Amazon Basin: Geology, https://doi.org/10.1130/G46319.1

Extended Methods

Study Site

Rivers draining the highly erodible Andean Cordillera yield the greatest amount of sediment to the adjacent lowlands of the foreland basins, on the order of 10^2 Mt of suspended material per river each year (Guyot et al., 1989; 1994; Latrubesse et al., 2005). Rivers with headwaters draining the fine-grained Neogene sedimentary rocks of the Central Amazon Trough yield an order of magnitude less sediment per river each year (Latrubesse et al., 2005), and those that drain the Brazilian Shield to the south of the Trough yield the least (Filizola and Guyot, 2009).

TSS fluxes within the tributaries of the Amazon include both sandy bed material, which is the material of bar formation, and silt-clay washload, which is transported through the channel and into floodplains without being sequestered onto bars. For the Amazon mainstem and seven of its tributaries, Dunne et al. (1998) calculated that bedload transport rates were <1% of total load, and the sandy bed-material transport was dominated by suspension; these are consistent with calculations based on grain-size and hydraulic measurements made by Aalto (2002). They also measured the annual suspended sand loads to comprise an average of 20% of TSS for both the mainstem Amazon and its tributaries (17% for tributaries with no or very small Andean sources). In our case. Such estimates are available for only one season in a single reach of an Amazonian tributary (Latrubesse et al., 2009).

Meander Symmetry Index (σ)

Each meander was defined as the reach length between inflection points (where the sign of planform curvature changes). Eroded-area polygons were constructed for each meander between the earliest and latest dates on record bounded by the inflection points at the primary time step. Eroded areas were then partitioned by the vertex intersecting the meander apex (where planform curvature reaches a maximum) at the primary time step, producing two portions of the meander, one for the upstream and one for the downstream portion. The ratio between the eroded-areas – calculated as the downstream eroded portion divided by the upstream eroded portion – defined a σ value for every meander present during the earliest image on record. New meanders or those that were terminated by cutoff were omitted from the analysis. Median σ values were used to classify the deformation style for each population of meanders along a reach. We adapted the descriptors defined by Daniel (1971) and Hooke (1984) to describe the dominant directional movement of the meander, in which $0.90 < \sigma < 1.05$ defined extension (i.e., orthogonal expansion of the meander), $\sigma < 0.90$ defined upstream rotation, and $\sigma > 1.05$ defined downstream rotation. Note, however, that each deformation descriptor does not preclude the other from contributing to the overall deformation of a single meander.

References Cited

Aalto, R.E., 2002, Geomorphic Form and Process of Sediment Flux Within an Active Orogen: Denudation of the Bolivian Andes and Sediment Conveyance Across the Beni Foreland: University of Washington, 364 p.

Constantine, J.A., and Dunne, T., 2008, Meander cutoff and the controls on the production of oxbow lakes: Geology, v. 36, p. 23–26, http://geology.gsapubs.org/content/36/1/23.abstract.

Constantine, J.A., Dunne, T., Ahmed, J., Legleiter, C., and Lazarus, E.D., 2014, Sediment supply as a driver of river meandering and floodplain evolution in the Amazon Basin: Nature Geosci, v. 7, p. 899–903, doi: 10.1038/ngeo2282 http://www.nature.com/ngeo/journal/v7/n12/abs/ngeo2282.html#supplementary-information.

Daniel, J.F., 1971, Channel movement of meandering Indiana streams: United States Geological Survey Professional Paper 732, v. A, p. 17.

Dunne, T., Mertes, L.A.K., Meade, R.H., Richey, J.E., and Forsberg, B.R., 1998, Exchanges of sediment between the flood plain and channel of the Amazon River in Brazil: Geological Society of America Bulletin, v. 110, p. 450–467.

Filizola, N., and Guyot, J.L., 2009, Suspended sediment yields in the Amazon basin: an assessment using the Brazilian national data set: Hydrological Processes, v. 23, p. 3207–3215, http://dx.doi.org/10.1002/hyp.7394.

Hooke, J.M., 1984, Changes in river meanders: Progress in Physical Geography, v. 8, p. 473–508, http://ppg.sagepub.com/content/8/4/473.short.

Latrubesse, E.M., Amsler, M.L., de Morais, R.P., and Aquino, S., 2009, The geomorphologic response of a large pristine alluvial river to tremendous deforestation in the South American tropics: The case of the Araguaia River: Geomorphology, v. 113, p. 239–252, doi: http://dx.doi.org/10.1016/j.geomorph.2009.03.014.

Latrubesse, E.M., Stevaux, J.C., and Sinha, R., 2005, Tropical rivers: Geomorphology, v. 70, p. 187–206, doi: 10.1016/j.geomorph.2005.02.005.

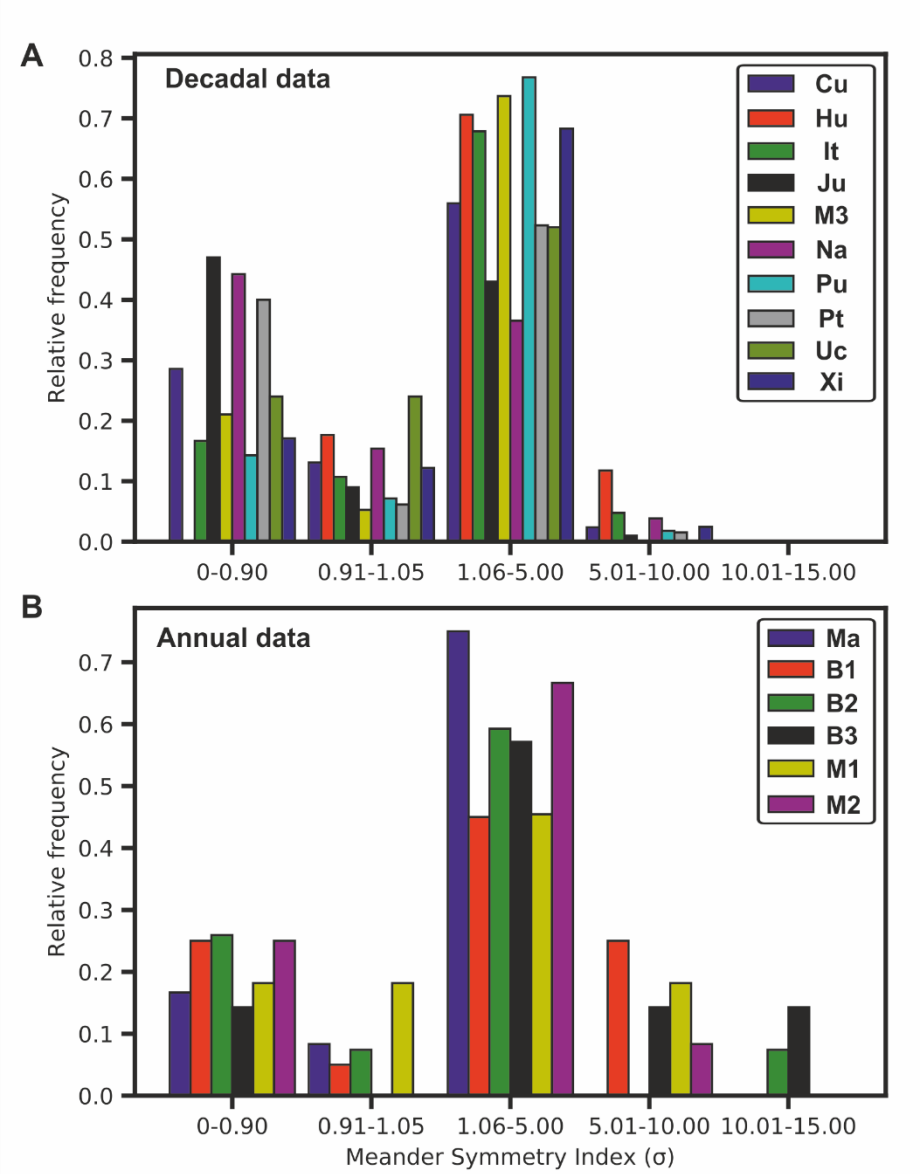

Figure DR1. Relative frequency distributions of σ-index for individual meanders along rivers covered by the A) decadal dataset, and B) annual dataset. The data was binned into upstream rotating meanders (0 – 0.90), extending meanders (0.90-1.05), and varying degrees of downstream rotating meanders (1.05-5; 5-10; 10-15). The rivers within each plot are symbolised and described by the legend.

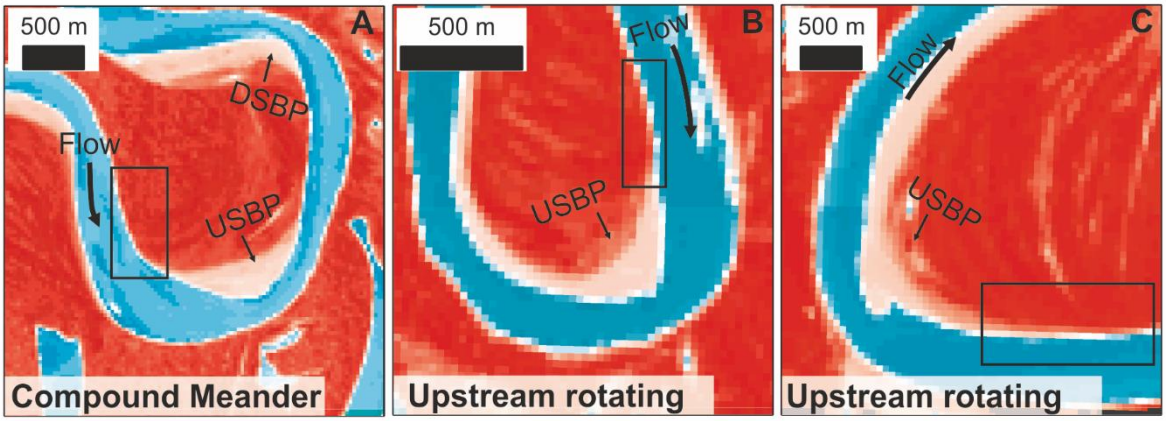

Figure DR2. Point bar positions in upstream rotating bends. Panel **A** shows a double-headed compound meander bend with point bars characterising each zone of curvature maxima. The bend moves predominantly downstream (downstream rotating); however, the upstream bar protrusion (USBP) is associated with localised channel widening. A downstream bar protrusion (DSBP) induces downstream meander rotation. Panels **B** and **C** illustrate bends experiencing upstream rotation (over the ~25-year observation period) and have clear examples of USBP. The black boxes indicate the absence of point bar deposits upstream of the bend apex consistent with experimental observations by Abad and Garcia (2009b) that revealed high velocity fluid is retained at the inner bank until experiencing curvature induced outward transport. Localised concentrations of sediment in the upstream portion of the meander will increase curvature and encourage outer bank retreat as the flow-field migrates outward across the channel. Panel **A** is taken from the R. Beni (-12.6 ^{O} N, -67.0 ^{O} W) while Panels **B** (-15.6^{O} N, -64.8 ^{O} W) and **C** (-15.3 ^{O} N, -64.9 ^{O} W) are from the R. Mamoré. All panels are displayed in modified NDVI format where the vegetation appears orange/red.

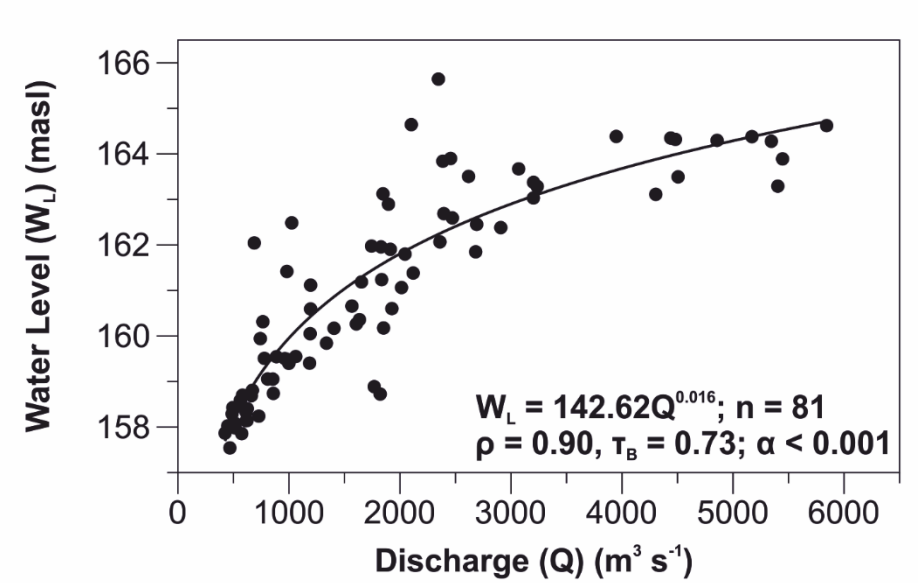

Figure DR3 Discharge plotted against estimated water level (W_L) at Rurrenabaque gauge. Water level estimates were obtained from SO-HyBAm (Observation Service for the Geodynamical, Hydrological, and Biogeochemical Control of Erosion/Alteration and Material Transport in the Amazon, Orinoco, and Congo Basins) collected using satellite altimetry. The measurements are subject to uncertainty associated with necessary atmospheric corrections and show an uncertainty of between 0.0050 and 0.13 m. Further information can be sourced from the SO-HyBAm website: http://www.ore-hybam.org/index.php/eng/Tecnicas/Station-limnimetrique-virtuelle.

Table DR1 Reach locations for both the decadal and annual datasets used in the study.

		Upstream limit		Downstream limit	
	Reach	Lat (decimal degrees)	Long (decimal degrees)	Lat (decimal degrees)	Long (decimal degrees)
Decadal Series	Xingu	-12.88	-52.82	-12.23	-53.30
	Jutai	-4.82	-68.56	-3.92	-67.72
	Itui	-5.12	-70.65	-4.65	-70.26
	Curuca	-5.10	-71.87	-4.45	-71.40
	Nanay	-3.90	-73.66	-3.70	-73.25
	Putumayo (Içа)	-2.36	-72.07	-3.14	-67.98
	Purus1	-7.82	-67.12	-7.54	-65.39
	Mamoré3	-14.92	-65.00	-13.72	-65.33
	Ucayali	-10.70	-73.77	-9.31	-74.40
	Huallaga	-5.79	-76.07	-5.17	-75.63
Annual Series	Beni1	-11.98	-66.90	-11.14	-66.15
	Beni2	-13.79	-67.53	-12.60	-66.95
	Beni3	-14.34	-67.56	-13.79	-67.53
	Mamoré1	-16.69	-64.81	-15.84	-64.74
	Mamoré2	-15.84	-64.74	-15.08	-65.00
	Madre de Díos	-11.53	-67.37	-11.01	-66.22

Table DR2 Equivalent total suspended sediment fluxes for each of the study reaches. Fluxes are to three significant figures and compiled from the literature. The original flux data can be sourced from the compilation presented by Constantine et al. (2014, Table S1). The data are divided into decadal and annual reaches.

	Reach	TSS (Mt m^{-1} yr^{-1})
Decadal series	Xingu	0.00174
	Jutai	0.00690
	Itui	0.00187
	Curuca	0.00194
	Nanay	0.00506
	Putumayo (Iça)	0.0333
	Purus	0.286
	Mamoré3	0.149
	Ucayali	0.342
	Huallaga	0.169
Annual series	Madre de Díos	0.113
	Beni1	0.471
	Beni2	0.573
	Beni3	0.505
	Mamoré1	0.0520
	Mamoré2	0.234

Table DR3. Measured parameters for Equation 2 used to calculate *S** for the decadally-resolved dataset. The variables measured from the Landsat imagery are taken from Constantine and Dunne (2008; Equation 4) and used to reformulate equation 1 in the present manuscript to equation 2. During reformulation the variables, *V, dS dt^{-1}*, and *dM dt^{-1}* are incorporated into *M**.

Reach Name	**dS dt^{-1}**	**Valley Length (V) (ch-w)**	**dn/dt (ch-w/yr)**	**L (ch-w)**	**f**	**dM/dt (ch-w yr^{-1})**	**S* (yr^{-1})**
Xingu	5.88E-04	559.44	0.00	0.00	0.00	0.329	0.00041
Jutai	1.11E-03	532.38	0.00	0.00	0.00	0.589	0.00052
Itui	-6.81E-04	467.52	1.12	18.88	0.86	0.805	0.00079
Curuca	2.57E-03	532.39	0.06	3.38	0.30	1.431	0.00118
Nanay	-1.64E-03	307.72	0.55	13.69	0.92	0.042	0.00006
Putumayo (Içа)	1.28E-04	713.61	0.00	0.00	0.00	0.091	0.00007
Purus	1.80E-03	584.20	2.17	31.30	0.90	3.227	0.00248
Mamoré3	-1.60E-03	344.91	2.51	10.48	0.52	1.964	0.00302
Ucayali	-1.75E-02	311.06	10.56	22.68	0.72	5.120	0.00782
Huallaga	5.58E-03	210.17	0.25	5.38	0.41	1.419	0.00417

‡ ***dS dt^{-1}*** *can be negative because negative length changes are associated with cutoffs.* However, ***S**** *excludes negative length changes associated with cutoffs.*

Table DR4 Meander symmetry indices (σ) for each study reach with number of meanders assessed (n), the reach-averaged σ-index and calculated lower and upper quartiles for each reach.

	Reach (n)	Median σ	25th Percentile	75th Percentile
Decadal series	**Xingu** *(41)*	1.24	1.01	1.51
	Jutai *(100)*	0.95	0.62	1.39
	Itui *(84)*	1.53	1.03	2.38
	Curuca *(84)*	1.17	0.78	1.63
	Nanay *(52)*	0.99	0.67	1.82
	Putumayo *(65)*	1.10	0.77	1.56
	Purus *(56)*	1.58	1.12	2.37
	Mamoré3 *(19)*	1.41	1.02	2.96
	Ucayali *(25)*	1.06	0.90	2.54
	Huallaga *(17)*	3.25	1.41	3.87
Annual series	**Madre de Díos** *(12)*	1.36	1.10	1.53
	Beni1 *(20)*	2.03	0.88	4.69
	Beni2 *(27)*	1.77	0.94	2.63
	Beni3 *(7)*	2.33	1.55	4.21
	Mamoré1 *(11)*	2.19	0.93	2.86
	Mamoré2 *(12)*	1.96	0.97	3.04

Table DR5 Subaerial bar extents for point bars displayed in Figure 4. Mean values are indicated by μ and geographical coordinates for the meanders are indicated in decimal degrees. Meanders A, B, and C correspond to the notations used in Figure 4. Changes in areal extent may result from imbalances between sediment erosion and deposition or variations in vegetation coverage and discharge. Estimates of river stage ($W_{L;}$ metres above sea level (masl)) between images are also given to account for differences in bar exposure when calculating bar areas. A rating curve was constructed from water stage and discharge data obtained from SO-HyBAm (**Fig. S3**). The curve was used to estimate water levels for the discharges recorded during each of the images displayed in Figure 4.

Meander	σ-index	Year						Meander location (Decimal Degrees)	
		1989	1996	1999	2004	2009			
		Bar area (km^2)					μ	Lat	Long
A	1.13	0.28	0.32	0.22	0.10	0.42	0.27	-12.8	-66.95
B	2.57	0.36	0.22	0.35	0.21	0.24	0.28	-12.89	-66.99
C	11.36	0.41	0.37	0.41	0.22	0.52	0.39	-13.09	-67.13
W_L		161.77	162.62	163.76	162.23	159.89			

Table DR6 Statistics associated with the correlations in Figures 2 and 3. The non-parametric statistics calculated for the data in each plot with associated confidence level (α) and number of observations (*n*).

Figure	***Statistic and correlation***	***Confidence level (α)***	***Number of observations (n)***
2A	Spearman's rank (ρ) = 0.80 Kendall's Tau (τ_B) = 0.60	α < 0.002	16
2B (Decadal data)	Spearman's rank (ρ) = 0.79 Kendall's Tau (τ_B) = 0.69	α < 0.0001	10
2B (Annual data)	Spearman's rank (ρ) = 0.85 Kendall's Tau (τ_B) = 0.67	α < 0.0001	271
3A	Spearman's rank (ρ) = 0.53 Kendall's Tau (τ_B) = 0.35	α < 0.06	16
3B	Spearman's rank (ρ) = 0.74 Kendall's Tau (τ_B) = 0.58	α < 0.002	16